Implications of low-energy fusion hindrance on stellar burning and nucleosynthesis

L. R. Gasques

Department of Nuclear Physics, Research School of Physical Sciences and Engineering, Australian National University, Canberra,
ACT 0200, Australia and Joint Institute for Nuclear Astrophysics, University of Notre Dame, Notre Dame, Indiana 46556, USA

E. F. Brown

Department of Physics & Astronomy and Joint Institute for Nuclear Astrophysics, National Superconducting Cyclotron Laboratory,
Michigan State University, East Lansing, Michigan 48824, USA

A. Chieffi

Istituto Nationale di Astrofisica, Osservatorio Astronomico di Roma, Via Frascati 33, I-00040 Monteporzio Catone, Italy

C. L. Jiang

Physics Division, Argonne National Laboratory, 9700 S. Cass Avenue, Argonne, Illinois 60439, USA

M. Limongi

Istituto Nationale di Astrofisica, Osservatorio Astronomico di Roma, Via Frascati 33, I-00040 Monteporzio Catone, Italy

C. Rolfs

Experimentalphysik III, Ruhr-Universität Bochum, Bochum, Germany

M. Wiescher

Department of Physics and Joint Institute for Nuclear Astrophysics, University of Notre Dame, Notre Dame, Indiana 46556, USA

D. G. Yakovlev

Ioffe Physical Technical Institute, Politekhnicheskaya 26, RU-194021 St.-Petersburg, Russia

We investigate the consequences of a new phenomenological model prediction of strongly reduced low-energy astrophysical S-factors for carbon and oxygen fusion reactions on stellar burning and nucleosynthesis. The new model drastically reduces the reaction rates in stellar matter at temperatures $T \lesssim (3\text{--}10) \times 10^8$ K, especially at densities $\rho \gtrsim 10^9$ g cm^{-3}, in a strongly screened or even pycnonuclear burning regime. We show that these modifications change the abundance of many isotopes in massive late-type stars and in particular strongly enhance the abundances of long-lived radioactive isotopes such as ^{26}Al and ^{60}Fe. The reduced reaction rates also significantly complicate carbon ignition (shift carbon ignition to higher temperatures and densities) in massive accreting white dwarfs exploding as type Ia supernovae and in accreting neutron stars producing superbursts. This would require much higher ignition densities for white dwarf supernovae and would widen the gulf between theoretical and inferred ignition depths for superbursts.

PACS number(s): 97.10.Cv, 97.10.Tk, 26.50.+x, 25.70.Jj

I. INTRODUCTION

Fusion reactions between ^{12}C and ^{16}O isotopes are crucially important in a wide variety of stellar burning scenarios. Recently, the reaction rates for the ^{12}C+^{12}C, ^{12}C+^{16}O, and ^{16}O+^{16}O fusion reactions have been re-evaluated [1,2]. These rates are sensitive to the reaction cross sections or astrophysical S-factors at low energies [3]. The experimental data are limited [4] to measurements of the fusion cross section above 2.4 MeV (center-of-mass energy) for the ^{12}C+^{12}C reaction, above 3.8 MeV for ^{12}C+^{16}O, and above 6.7 MeV for the ^{16}O+^{16}O reaction. To determine a reliable reaction rate in stellar matter, experimental S-factors must be extrapolated to lower energies.

The goal of the previous work [1,2] was to improve the low-energy S-factor parametrization of Fowler, Caughlan, and Zimmermann [5] and of Caughlan and Fowler [6] by extrapolating the S-factor data in the framework of the theoretical São Paulo potential model. The resulting thermonuclear reaction rates show overall good agreement with the previous compilations [5,6].

In recent years, an unexpected hindrance of heavy-ion fusion cross sections, in comparison to single- and coupled-channels model calculations, has been observed at sub-barrier bombarding energies [7–12]. The consequence of this hindrance is a significant reduction of the astrophysical S-factors at lower energies. This phenomenon was first reported for fusion reactions of medium-heavy nuclei, $A \gtrsim 50$. Indications for such a behavior have also been found in reactions involving some lighter nuclei. This includes the reactions of significant astrophysical relevance such as ^{12}C+^{12}C, ^{12}C+^{16}O, and ^{16}O+^{16}O [12]. No evidence of the hindrance effect has been

observed in reactions involving nuclei lighter than ^{10}B. In a recent publication, Mişicu and Esbensen [13] demonstrated that the low-energy fusion hindrance can be explained by introducing a shallow ion-ion potential related to the incompressibility of nuclear matter. In particular, these calculations can reproduce the hindrance effect in experimentally measured cross sections for the ^{64}Ni+^{64}Ni, ^{28}Si+^{64}Ni, and ^{64}Ni+^{100}Mo reactions [8,14,15].

In this article, we explore the astrophysical consequences of a possible hindrance effect [12] on the S-factors of the reactions ^{12}C+^{12}C, ^{12}C+^{16}O, and ^{16}O+^{16}O. These reactions are important for the evolution of post-main sequence stars and the associated nucleosynthesis. In addition, the ignition of ^{12}C+^{12}C triggers type Ia supernovae in accreting carbon-oxygen white dwarfs. It is also proposed as a trigger for the recently discovered superbursts on the surface of accreting neutron stars. In the following, we first (Sec. II) describe how the hindrance in the S-factor reduces the carbon and oxygen reaction rates at stellar energies. We then explore the consequences of the hindrance on the evolution of massive stars (Sec. III). We further demonstrate the impact of the proposed hindrance on explosive ignition of ^{12}C in white dwarfs (Sec. IV A) and neutron stars (Sec. IV B) before concluding in Sec. V.

II. FUSION RATES AT STELLAR ENERGIES

Recently Jiang *et al.* [12] pointed out a possible impact of the hindrance on the S-factor for the ^{12}C+^{12}C, ^{12}C+^{16}O, and ^{16}O+^{16}O reactions at sub-barrier center-of-mass collision energies E. They proposed a corresponding parametrization for the energy dependence $S(E)$ based on the assumption that the logarithmic derivative $L(E) = d[\ln(E\sigma)]/dE$ of the fusion cross-section $\sigma(E)$ depends on E as $L(E) = A_0 + B_0/E^{3/2}$. They determined A_0 and B_0, in the framework of their model, by fitting the values of $L(E)$ extracted from experimental data at energies below the Coulomb barrier.

The results are shown in Fig. 1. The upper panels present the experimental S-factors for the discussed reactions versus E in comparison with previous predictions by Fowler *et al.* [5,6], Yakovlev *et al.* [2], and the new predictions by Jiang *et al.* [12]. Different symbols indicate the various experimental data sets. For a better presentation, the data of each set are binned into $\Delta E = 0.5$ MeV energy intervals. Thick solid lines (labeled as "Standard") and thick dashed lines ("Standard1") are the standard predictions of Ref. [2] and [5,6], respectively. Thin solid lines represent the reduced S-factors [12]. They are plotted to maximum energies of 5.8 MeV (^{12}C+^{12}C), 6.0 MeV (^{12}C+^{16}O), and 8.5 MeV (^{16}O+^{16}O) to which the fits [12] were constructed. At higher E the results of Ref. [12] are meant to coincide with the standard predictions [5,6].

The experimental data for the ^{12}C+^{12}C reaction in the left upper panel of Fig. 1 have been taken from Patterson *et al.* [16], Mazarakis and Stephens [17], and High and Cujec [18]. Also shown are the data of Kettner *et al.* [19], Becker *et al.* [20], Erb and Bromley [21], Dasmahapatra *et al.* [22], and Satkowiak *et al.* [23], which were not included in Fig. 8b of Jiang *et al.* [12] (because the energies of those measurements are higher

than the energies at which the hindrance effect is pronounced). In addition, we plot more recent data of Rosales *et al.* [24], Aguilera *et al.* [25], Barrón-Palos *et al.* [26], and the most recent data of Spillane *et al.* [27]. The data reveal narrow resonance structures that have been associated [28] with quasi-molecular states in the ^{12}C+^{12}C system. These resonances cannot be described by the potential models discussed here that only seek to reproduce an overall energy dependence $S(E)$.

The middle and right upper panels of Fig. 1 display $S(E)$ for the ^{12}C+^{16}O and ^{16}O+^{16}O reactions, respectively. Experimental data are from Ref. [29,30] for the ^{12}C+^{16}O and from [31–36] for the ^{16}O+^{16}O process. They are the same as shown in Figs. 6b and 3b of Jiang *et al.* [12].

The "standard" theoretical calculations of Refs. [5,6] and [1,2] describe well the experimental data and predict an increase in $S(E)$ toward lower energies of the stellar burning range. In contrast, the hindrance phenomenon [12] predicts a maximum of $S(E)$ followed by a decrease toward lower energies. For the given reactions, the standard and reduced low-energy $S(E)$ predictions have comparable statistical significance. One cannot discriminate between the standard and reduced concepts of carbon and oxygen burning using current experimental data. Only the standard S-factors have been employed so far in astrophysical implications.

In the following we focus on the consequences of the strong reduction of $S(E)$ at low E predicted by the hindrance effect. The effect modifies the reaction rates R in stellar matter as illustrated in the middle and bottom panels of Fig. 1. The middle panels show the normalized thermonuclear ^{12}C+^{12}C, ^{12}C+^{16}O, and ^{16}O+^{16}O reaction rates

$$N_A \langle \sigma v \rangle = 4 N_A \sqrt{\frac{2E_0}{3\mu}} \frac{S(E_0)}{kT} \exp(-\tau), \qquad (1)$$

where $E_0 = kT\tau/3$ is the Gamow-peak energy, k is the Boltzmann constant, μ is the reduced mass of colliding nuclei, $\tau = [27\pi^2 \mu Z_1^2 Z_2^2 e^4/(2kT\hbar^2)]^{1/3}$, N_A is Avogadro's number, and Z_1 and Z_2 are charge numbers of the nuclei. Furthermore, v is the relative velocity of the nuclei, and $\langle \sigma v \rangle$ denotes the averaging of σv over the Maxwellian distribution of the relative velocities. The S-factors are assumed to be slowly varying functions of E (on energy scales of the order of the Gamow-peak widths; see, e.g., Ref. [2]). The effects of plasma screening [37] on the normalized reaction rates are neglected, which is justified at sufficiently high T, at which Coulomb coupling of the nuclei is weak $[T \gtrsim T_l = Z_1 Z_2 e^2/ka_{12}$, where $a_{12} = (a_1 + a_2)/2$; $a_1 = a_e Z_1^{1/3}$ and $a_2 = a_e Z_2^{1/3}$ are ion sphere radii determined by the electron sphere radius $a_e = (3/4\pi n_e)^{1/3}$; n_e is the electron number density $n_e]$. The normalized reaction rates are related to the actual rates $R = n_1 n_2 \langle \sigma v \rangle \delta$, where n_1 and n_2 are the number densities of the reacting nuclei, and δ is the symmetry factor ($\delta = 1/2$ and 1 for reactions with identical and different nuclei, respectively).

The normalized reaction rates defined by Eq. (1) are independent of density and composition of stellar matter but depend on T. This temperature dependence is plotted in the middle panels of Fig. 1 for the same standard and reduced theoretical S-factor models as in the upper panels. We see that both standard S-factor models give very similar
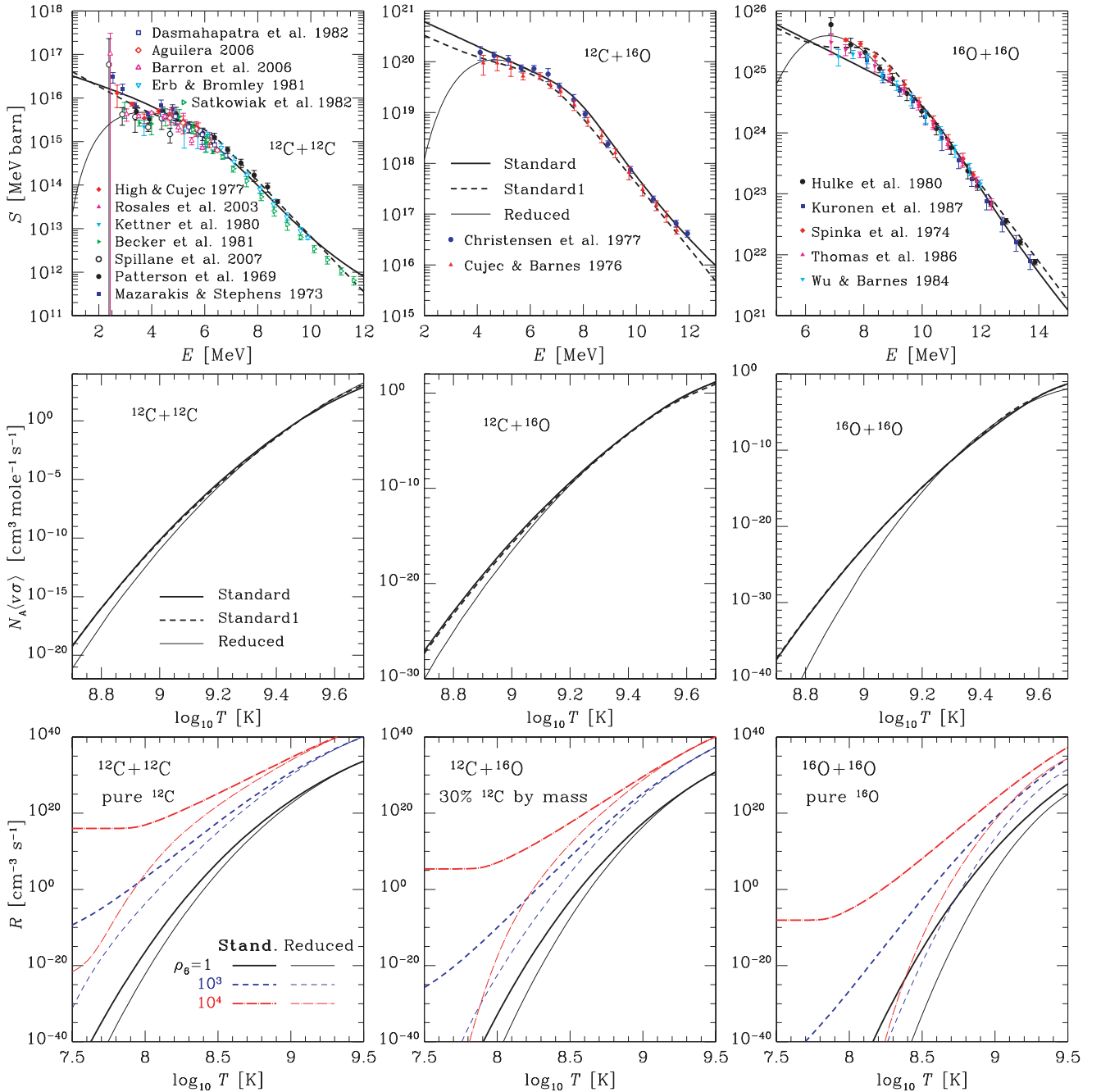
FIG. 1. (Color online) (Top) Astrophysical factors for the ^{12}C+^{12}C, ^{12}C+^{16}O, and ^{16}O+^{16}O reactions versus center-of-mass energy E of colliding nuclei. Various symbols show experimental data. (Middle) Normalized rates of these reactions versus temperature neglecting plasma screening effects. (Bottom) Rates of the same reactions versus temperature for three values of the density ($\rho = 10^6$, 10^9, and 10^{10} g cm^{-3}, $\rho_6 \equiv \rho/10^6$ g cm^{-3}) in pure carbon matter (left), in a C-O mixture with 30% of carbon by mass (middle), and in pure oxygen matter (right). Thick lines refer to standard S-factors (either recent model calculations [1,2], denoted as Standard, or the formalism of Fowler *et al.* [5,6]. denoted as Standard1); thin lines refer to reduced S-factors (Jiang *et al.* [12]). See text for details.

reaction rates (being based on the same physical assumptions). The reduced S-factors lead to nearly the same rates at $T \gtrsim 2 \times 10^9$ K but suppress the rates at lower T because of the hindrance effect. Notice that at these lower T the reduced S-factors, which contribute to the reaction rates, become rapidly varying functions of E. Strictly speaking, such a rapid energy dependence should modify the classical expression,

Eq. (1). We have checked that the effect is not too strong. For instance, it enhances the normalized reduced ^{12}C+^{12}C reaction rate at $T = 10^{8.7}$ K (the left middle panel in Fig. 1) by only $\approx$30%. Accordingly, we neglect this effect throughout this article.

The three lower panels of Fig. 1 show the temperature dependence of the ^{12}C+^{12}C, ^{12}C+^{16}O, and ^{16}O+^{16}O reaction

rates R, which depend on T, the density ρ, and the composition of the matter. The ^{12}C+^{12}C reaction is considered in pure carbon matter, the ^{16}O+^{16}O reaction in pure oxygen matter, and the ^{12}C+^{16}O reaction in a carbon-oxygen mixture with 30% carbon by mass. Each panel presents R for three values of the density, $\rho = 10^6$, 10^9, and 10^{10} g cm^{-3} (solid, dashed, and dot-dashed lines, respectively). The effects of dense matter on Coulomb tunneling in nuclear reactions are included in accordance with the "optimal" (most realistic) Coulomb tunneling model of Ref. [2]. Thick lines are for the "Standard" astrophysical factor $S(E)$ model, whereas thin lines are for the reduced $S(E)$ model. The results for the "Standard" and "Standard1" models are close, and we therefore do not plot the "Standard1" curves.

The complicated behavior of the R curves reflects a variety of nuclear burning regimes (the importance of plasma screening and pycnonuclear effects in nuclear reactions as described, e.g., in Refs. [2,37]). Plasma screening is efficient and strongly enhances the reaction rates at intermediate $T \lesssim T_l$, for which Coulomb ion coupling becomes strong (see above). For $\rho = 10^6$ g cm^{-3} this happens at $T \lesssim (3-6) \times 10^8$ K for the reactions of study. For $\rho = 10^9$ g cm^{-3} the plasma screening becomes strong at $T \lesssim (3-6) \times 10^9$ K and for $\rho = 10^{10}$ g cm^{-3} at even higher T (is strong for all T shown in Fig. 1). The pycnonuclear effects are pronounced at lower temperatures $T \lesssim T_p$, where $T_p = \hbar\omega_p/k$ and ω_p is the ion plasma frequency. We have $T_p \sim 4 \times 10^6$, 10^8, and 4×10^8 K for $\rho = 10^6$, 10^9, and 10^{10} g cm^{-3}, respectively. When T decreases much below T_p, thermonuclear burning transforms into pycnonuclear burning, and the reaction rate becomes independent of temperature. In this regime the rate is rather uncertain because of theoretical uncertainties of the Coulomb tunneling problem (e.g., Refs. [1,2]). In the displayed temperature range the pycnonuclear effects are most pronounced at $\rho \sim 10^{10}$ g cm^{-3}. The strongest hindrance effect on the reaction rates takes place in the pycnonuclear regime because the energies of nuclei contributing to the reaction rates are especially low in this regime. Both reaction rate predictions are based on extrapolations that may break down at such low energies. For instance, the hindrance effect reduces the standard pycnonuclear ^{12}C+^{12}C reaction rate at $\rho \sim 10^{10}$ g cm^{-3} by nearly 40 orders of magnitude. This enormous reduction should be regarded with caution because it is based on the extrapolation of the parametrized S-factor [12] to very low energies ($E \sim 30$ keV). The parametrization itself is built on the experimental data in the range from $E = 2.4$ to 5.8 MeV; it predicts an exponential decrease of $S(E)$ with decreasing E and becomes, therefore, very risky at $E \sim 30$ keV.

Let us emphasize that the hindrance uncertainties of the reaction rates are much stronger than the uncertainties associated with the plasma physics problems of quantum tunneling for fusing nuclei in dense matter. For instance, according to Fig. 4 of Ref. [2], the plasma physics uncertainties of the ^{12}C+^{12}C pycnonuclear burning rate at $\rho \sim 10^{10}$ g cm^{-3} reach nearly 10 orders of magnitude, which is much smaller than the uncertainties related to the hindrance of heavy-ion fusion cross sections ($\sim$40 orders of magnitude). Experimental

data indicate also the presence of resonance structures in $S(E)$ (see the upper panels of Fig. 1) which are usually neglected in astrophysical applications. It can be shown that the resonant structures for the reactions of our interest, detected at present (e.g., at $E > 2.4$ MeV for the ^{12}C+^{12}C reaction), are smeared out within the Gamow-peak energy range and thus hardly affect the reaction rates (see Ref. [2], particularly Fig. 1 there). The problem of resonances at low energies remains open but it is unlikely that they would be more important than the hindrance effect in the reaction rate calculations.

In the following two sections we discuss possible consequences of the hindrance on the evolution of massive stars and on carbon ignition in accreting white dwarfs and neutron stars.

III. EVOLUTION OF HIGH-MASS STARS

Carbon burning in evolved massive stars $M = (15-60)\,M_\odot$ ($M_\odot$ being the solar mass) takes place at temperatures $T \approx (5-10) \times 10^8$ K and densities $\rho \approx (10^4-10^5)$ g cm^{-3} [38,39]. Oxygen burning requires higher temperatures to overcome the larger Coulomb barrier; it occurs at $T \approx (1-3) \times 10^9$ K and $\rho \approx (10^6-10^7)$ g cm^{-3}. Under these conditions, the plasma screening and pycnonuclear burning are not important, but the difference between standard and reduced reaction rates is pronounced (up to two orders of magnitude at lower temperatures in the left middle panel of Fig. 1).

We calculated the nucleosynthesis following the stellar evolution (hydrogen, helium, and all more advanced burning stages) and subsequent supernova explosion of two massive stars, with $M = 20$ and $60\,M_\odot$ and an initial solar abundance distribution. We used the latest version of the FRANEC code as described by Limongi and Chieffi [40]. The nuclear network includes 267 isotopes (from neutrons to ^{98}Mo) and about 3000 reactions. The network is fully coupled to the equations that describe the structure of the star; the equations of physical and nuclear evolution have been solved simultaneously. We employed either the standard ^{12}C+^{12}C, ^{12}C+^{16}O, ^{16}O+^{16}O reaction rates of Fowler *et al.* [5,6] or the reduced reaction rates of Jiang *et al.* [12]; otherwise the physics input is the same. The results for the standard reaction rates [2] are nearly identical to the ones based on the rates by Fowler *et al.* [5,6] (see Sec. II and middle panels of Fig. 1) and are therefore not presented here.

Figure 2 shows deviations in the final abundances of stable nuclei in the mass range from ^{12}C to ^{98}Mo for the $20\,M_\odot$ and $60\,M_\odot$ models. The figure reflects the integrated impact of the reduced rates. For the $20\,M_\odot$ star, the hindrance effect reduces the abundances of ^{40}Ca, ^{46}Ti, and ^{50}Cr by $\approx$50%. In contrast, it enhances the abundances of ^{46}Ca and ^{84}Sr by a factor of 2 and 4, respectively. The hindrance effects on the evolution of the $60\,M_\odot$ star are weaker. This is because the ^{12}C abundance created during He burning declines with increasing stellar mass [38] and the importance of carbon burning is largely reduced.

Figure 3 shows the abundance distribution over the inner core of the $20\,M_\odot$ star at different burning stages for both the standard and reduced fusion rates (M being a Lagrangian mass coordinate within the star). We present the abundances of
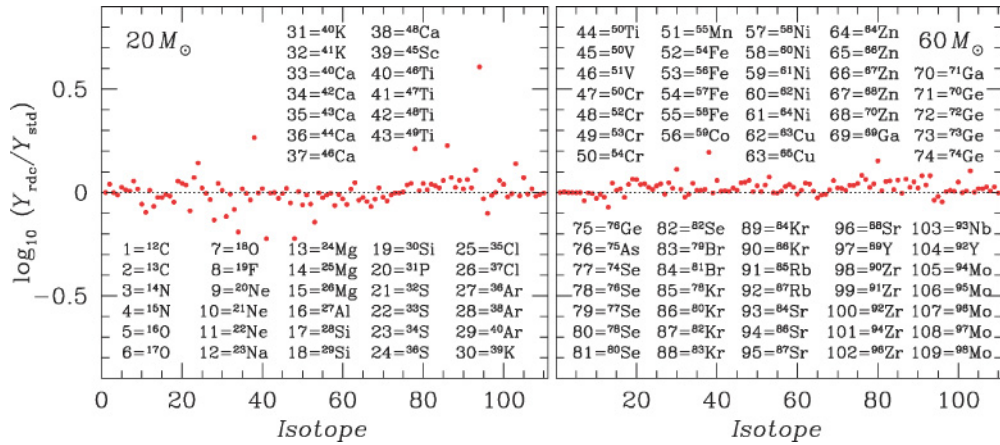
FIG. 2. (Color online) Deviations in isotopic abundances Y_{rdc} for the reduced fusion rates from the abundances Y_{std} for the standard rates [5,6] at the endpoint of evolution of 20 $M_\odot$ (left) and 60 $M_\odot$ (right) stars. Shown are the abundances of 109 isotopes 1...109 from ^{12}C to ^{98}Mo.

selected isotopes between ^{1}H and ^{60}Fe at six evolution stages. These are exhaustion of carbon core burning, carbon shell burning, ignition and exhaustion of core neon burning, as well as ignition and exhaustion of core oxygen burning. In addition to the abundances of light seed isotopes such as ^{1}H, ^{4}He, ^{12}C, and ^{16}C we display the directly associated abundances of ^{20}Ne, ^{22}Ne, ^{24}Mg, ^{25}Mg, and ^{28}Si. The thick solid lines refer to the standard fusion rates, whereas the light dashed lines are

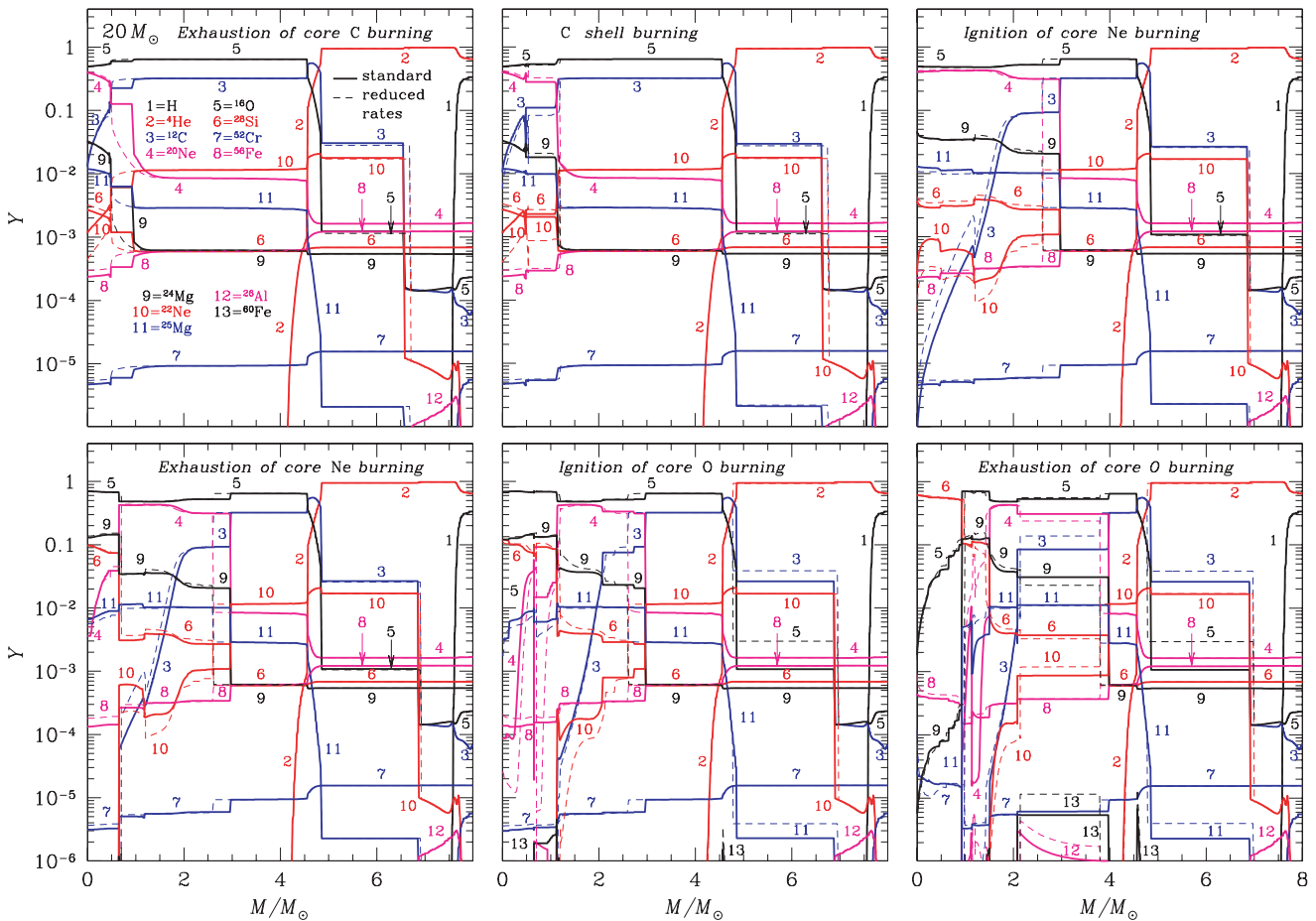

FIG. 3. (Color online) Abundance distributions of selected isotopes between ^{1}H and ^{60}Fe for the core and shell burning zones at different late evolution stages of the 20 $M_\odot$ star. The thick solid lines correspond to the standard fusion rates, whereas the thin dashed lines are for the reduced rates. See text for details.
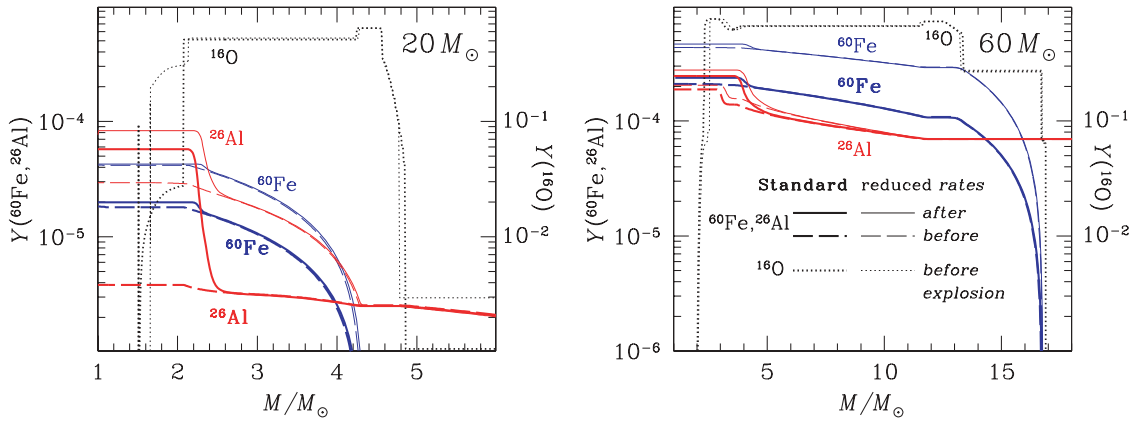
FIG. 4. (Color online) Abundance distribution of the long-lived radioactive isotopes ^{26}Al and ^{60}Fe (left vertical scales) over the inner core and shell burning zones of 20 $M_\odot$ and 60 $M_\odot$ stars. The dashed and solid lines show the abundances at the end of stellar evolution and after passage of a shock induced by explosive burning, respectively. The dotted lines display the oxygen abundance (right vertical scales) before the shock passage. Thick lines are calculated with the standard reaction rates; thin lines are for the reduced rates.

calculated with the reduced rates. Note also the appearance of neutrons produced by the ^{13}C(α, n) or ^{22}Ne(α, n) reactions. We show the abundances of heavier isotopes produced by subsequent neutron or proton and α captures of light fusion products. This includes ^{52}Cr and ^{56}Fe as well as long-lived γ emitters ^{26}Al and ^{60}Fe, which have been predicted [41] to be produced in copious amounts in massive stars.

According to Fig. 3, in most cases the differences in isotope abundances for the standard and reduced reaction rates are relatively small. They mainly occur near the fringes of the shell regions or at intershell zones. A comparison of the abundances at the exhaustion of carbon core burning and during shell carbon burning indicates differences mainly for the carbon distribution in the emerging shell that extends much deeper for the reduced rates. Also affected is the neon distribution in the remaining core, which is much more extended toward lower core masses for the standard fusion rates, as a result of a faster standard carbon burning at given temperatures.

The main difference in the abundances for the standard and reduced fusion rates during ignition and after the subsequent phase of core neon burning is in the neutron distribution (not shown in Fig. 3). Also the oxygen content at the bottom of the carbon shell is slightly higher for the reduced fusion rates.

During the ignition and after the phase of core oxygen burning, considerable temperature difference occurs in the inner core and in shell regions at the onset of oxygen burning, translating into a significantly higher neutron production for the reduced fusion model. Notable is also the enhancement in ^{16}O versus the reduction in ^{20}Ne in the neon burning shell after the exhaustion of core oxygen burning. The increase in neutron production translates into much higher ^{26}Al and ^{60}Fe abundances using the reduced fusion rates. This enhancement of long-lived radio isotopes is the most notable change; the enhancement of ^{26}Al would indeed match the observed ^{26}Al abundance in our galaxy that is higher than predicted by the present nucleosynthesis models [41]. However, the enhanced ^{60}Fe production provided by the new reduced fusion rates would further enhance the already overpredicted ^{60}Fe abundance in the galaxy.

Figure 4 shows the cumulative abundance of ^{26}Al and ^{60}Fe for the 20 $M_\odot$ and 60 $M_\odot$ stars. The solid lines refer to the final abundances after the passage of the shock wave, whereas the dashed ones refer to the abundances before the shock passage. For reference, the dotted lines display the ^{16}O abundance at the beginning of the core collapse. They clearly show the location of both the O-shell and the C-convective shell at the beginning of the core collapse.

In the 20 $M_\odot$ star (left panel in Fig. 4) the difference between the standard and reduced fusion rates is visible in the carbon convective shell for both ^{26}Al and ^{60}Fe (the contribution of the Ne explosive burning is similar for the two fusion rates). The two convective shells differ because carbon burning with the reduced rates requires higher temperatures. This temperature increase is sufficiently small to maintain the abundance of the main products of the burning but large enough to increase the neutron and proton production in the carbon convective shell. As a result, the reduced rates significantly affect the abundance of not only ^{26}Al and ^{60}Fe but also of ^{46}Ca, ^{74}Se, ^{78}Kr, and ^{84}Sr (see Fig. 2).

In the 60 $M_\odot$ star (right panel in Fig. 4) the differences in the carbon convective shell are smaller. Most notably, no enhancement is observed for neutron-deficient isotopes (such as ^{26}Al) because the amount of carbon left by the He burning is much smaller than in the 20 $M_\odot$ star. Therefore, the difference in the standard and reduced fusion rates is less important for temperatures in the carbon burning shell. However, there is a huge difference in the ^{60}Fe produced in the He shell. The reason is once again that this ^{60}Fe is extremely sensitive to the neutron density provided by the temperature-dependent ^{22}Ne$(\alpha, n)^{25}$Mg reaction. Because carbon burning with the reduced rates requires higher temperatures, the base of the helium convective shell is slightly hotter, increasing neutron production and enhancing subsequently the ^{46}Ca and ^{60}Fe abundance.

The overall influence of the changes in the ^{16}O$+^{16}$O and ^{12}C$+^{16}$O rates is much weaker because the matter processed by oxygen burning is later fully reprocessed by the explosive burning at the supernova shock front.

IV. CARBON IGNITION IN DENSE STELLAR MATTER

An important problem is the fate of dense matter undergoing compression in the cores of accreting white dwarfs and the crusts of accreting neutron stars. Here we outline carbon ignition in this matter, which in the core of a massive white dwarf leads to a type Ia supernova and in the crust of a neutron star leads to a superburst. Following ([42,43]) we will write the condition for unstable carbon burning in the form

$$(\partial \epsilon_{\mathrm{nuc}}/\partial T)_P - (\partial \epsilon_{\mathrm{cool}}/\partial T)_P > 0, \qquad (2)$$

where ϵ_{nuc} is the nuclear energy generation rate (per gram) in the ^{12}C+^{12}C process, whereas $\epsilon_{\mathrm{cool}} = \epsilon_\nu + \epsilon_{\mathrm{cond}}$ is the cooling rate (that includes neutrino cooling ϵ_ν and thermal conduction cooling ϵ_{cond}). Derivatives have to be taken at constant pressure P. Carbon ignition occurs at those P and T at which Eq. (2) equals zero.

A. Ignition of type Ia supernova explosions

It is widely accepted that type Ia supernova explosions are triggered by carbon ignition in central regions of massive accreting white dwarfs [44,45]. The ignition curve is calculated on the basis of Eq. (2) with $\epsilon_{\mathrm{cool}} = \epsilon_\nu$ (because neutrino cooling is much more efficient than thermal conduction in white dwarf cores). The neutrino emission in white dwarfs is mainly provided by plasmon decay and electron-nucleus bremsstrahlung (calculated as prescribed in Ref. [2]).

The standard carbon ignition curve $T_{\mathrm{ign}}(\rho)$ is plotted by the thick dot-dash line in Fig. 5. It is calculated using the carbon fusion rates from Ref. [2] for a ^{12}C-^{16}O mixture with 30% of carbon by mass (a fiducial value for massive carbon-oxygen white dwarfs; see, e.g., Ref. [46]). Carbon burning is stable for ρ and T below this curve and unstable above it. The curve is nearly horizontal at $\rho \lesssim 10^9$ g cm^{-3} because at these densities the ignition occurs in thermonuclear burning regime (with strong plasma screening); see Sec. I and the lower panels of Fig. 1. A strong decline of the curve at $\rho \gtrsim 10^9$ g cm^{-3} signals the beginning of a transition to pycnonuclear burning. According to the standard fusion results, the ignition in the core of a massive white dwarf occurs at $\rho \sim (2$–$4) \times 10^9$ g cm^{-3} and $T_{\mathrm{ign}}(\rho)$ a few times of 10^8 K. The initial ignition stage is slow because generated nuclear energy is spent to initiate strong convection in the white dwarf core. It takes centuries before the temperature reaches $T \sim 7 \times 10^8$ K and the white dwarf finally explodes (see, e.g., Ref. [47]).

The thin dash-and-dot line in Fig. 5 presents the same carbon ignition curve but for the reduced carbon fusion rate. The ignition temperature $T_{\mathrm{ign}}(\rho)$ is generally higher than in the standard scenario because of strongly suppressed fusion (also see lower panels of Fig. 1). The most dramatic difference occurs at higher densities, $\rho \gtrsim 10^{10}$ g cm^{-3}. In this case the standard ignition curve becomes nearly vertical [2] because of the strong pycnonuclear burning, whereas the new curve declines very slowly. Notice that carbon and oxygen cannot survive at $\rho \gtrsim (2$–$4) \times 10^{10}$ g cm^{-3} because of β captures. We therefore do not extend the ignition curve to these unphysical higher densities.

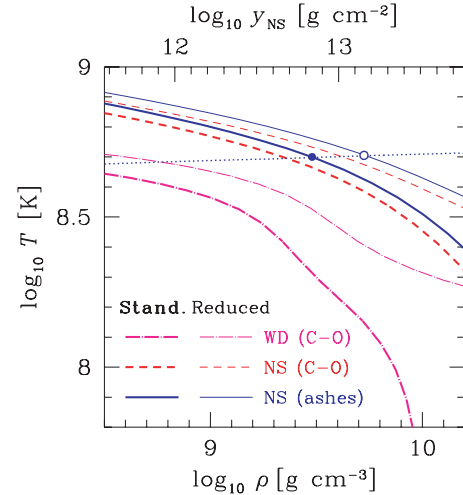FIG. 5. (Color online) Carbon ignition curves in a core of a massive ^{12}C-^{16}O white dwarf (WD; 30% of carbon by mass), in a neutron star (NS) crust with the same composition (dashed lines), and in a neutron star crust containing mixture of ashes of hydrogen and helium burning (solid lines). Thick lines refer to standard carbon burning rate, whereas thin lines are for the reduced rate. The upper axis gives the column depth $y_{\mathrm{NS}} = P/g$ within a crust of an accreting $1.6\,M_\odot$ neutron star with the radius of 10.8 km. The dotted line is a temperature profile within the crust of such a star assuming the crust is composed of ashes and the accretion rate ≈ 0.3 of the Eddington rate. The filled and open dots position carbon ignition in such a crust for the standard and reduced carbon fusion rates, respectively. See text for details.

As seen from Fig. 5, the hindrance of the carbon fusion rate will strongly delay carbon ignition in white dwarfs by shifting the ignition to higher densities and temperatures. For instance, for the ignition to start at $\rho \approx 2 \times 10^9$ g cm^{-3}, the white dwarf core should be heated up to $T \approx 2.8 \times 10^8$ K in the standard scenario but to $\approx 4 \times 10^8$ K for the reduced rates. This difference in ignition temperatures leads to drastically different physical conditions; the whole dynamics from the initial ignition to the supernova explosion with the new rates should be reconsidered. If the temperature of the white dwarf core is lower than $\sim 2 \times 10^8$ K, carbon can still ignite at sufficiently high ρ in the standard scenario but cannot ignite at all with the reduced rates. Notice that these conclusions are based on the extrapolations of the S-factor data measured at much higher energies (Sec. II). Changes in the assumed carbon abundance (30% by mass) will have only a minor impact on the results discussed here. The uncertainties of the Coulomb tunneling problem in dense matter also affect the carbon ignition curve, resulting in much weaker influence on the reaction rates than the hindrance effect (see Refs. [1,2], where plasma physics uncertainties in carbon ignition are studied for the standard reaction rates).

B. Ignition conditions of superbursts

Explosive carbon burning in the outer crust of an accreting neutron star is thought to power superbursts ([43,48,49]). Superbursts are energetic ($\sim 10^{42}$ erg), long ($\sim$ hours) x-ray

flares observed from accreting neutron stars (for a summary of observations, see Ref. [50]). The ignition conditions depend critically on the thermal structure of the outer crust.

Examples of carbon ignition curves in a crust of a neutron star of mass $M = 1.6 M_\odot$ and radius 10.8 km are shown by solid and dashed lines in Fig. 5. They are calculated on the basis of Eq. (2) using the same model for the carbon fusion rate as in Sec. IV A. The thick and thin lines refer to the standard and reduced rates, respectively. In contrast to white dwarf cores, the cooling term is now dominated by thermal conduction, so that $\epsilon_{cool} \approx \epsilon_{cond}$ in Eq. (2). The thermal conduction term has been computed in a one-zone approximation of the thermal diffusion equation ([42,43]) as $\epsilon_{cool} = \rho K T / y^2$, which is the finite-difference estimate of the divergence of the heat flux, with K being the thermal conductivity, $y = P/g$ the column depth, and g the surface gravity. The upper horizontal axis in Fig. 5 shows the column depth $y = y_{NS}$ for the given neutron star model.

The carbon ignition temperatures $T_{ign}(\rho)$ in neutron star crusts are higher than in white dwarfs because the efficient thermal conduction in the crust stabilizes carbon burning at higher T and ρ. Carbon ignition in neutron stars occurs in the thermonuclear regime with strong plasma screening. The difference of the ignition curves calculated for the standard and reduced rates is smaller but nevertheless pronounced.

The dashed ignition curves are calculated for the same ^{12}C-^{16}O mixture with 30% carbon by mass as for white dwarfs. Such a composition is not realistic for matter in the accreted neutron star ocean but allows a direct comparison of the ignition curves in neutron stars and white dwarfs with the same composition of the matter. For instance, the standard ignition temperature at $\rho \approx 2 \times 10^9$ g cm^{-3} in a neutron star is $\approx 5.5 \times 10^8$ K versus $\approx 2.8 \times 10^8$ K in a white dwarf. The difference in ignition temperature reflects the difference in cooling mechanisms—neutrino emission from the core versus thermal conduction in a thin surface layer—for type Ia supernovae and superbursts. In addition, the combustion front in a superburst ignites in a region of strong gravitational acceleration, which greatly affects the dynamics of the burn [51].

The solid ignition curves in Fig. 5 are computed for a plausible superburst fuel mixture, the ashes of *stable* hydrogen and helium burning [52]. This mixture contains 8% by mass of ^{12}C, with the remainder being mostly ^{56}Cr (36% by mass), ^{57}Co and ^{57}Fe (8% by mass together), ^{58}Ni (6%), and ^{60}Ni (5%). These ignition temperatures are higher than the corresponding temperatures for the carbon-oxygen mixture because of the smaller amount of carbon and, hence, smaller carbon burning rate in the ashes. In addition, in Fig. 5 we show the temperature profile $T(y)$ computed by Gupta *et al.* [53] for the neutron-star crust composed of ashes. It is assumed that the star accretes locally at a rate of 2.1×10^4 g s^{-1} cm^{-2} (≈ 0.3 Eddington accretion rate). Carbon ignites at those values of ρ and T at which the temperature profile intersects an ignition curve. For the standard and reduced fusion rates such ignition points are shown by filled and open dots, respectively. We find that the reduced fusion rate increases the ignition column depth y_{ign} by about a factor of 2, from $y_{ign} = 8 \times 10^{12}$ g cm^{-2} to $y_{ign} = 1.8 \times 10^{13}$ g cm^{-2}.

However, the ignition depths can be inferred from observations. Cumming *et al.* [54] showed that the decay of the superburst lightcurve can be well fitted by a broken power law, with the break indicating the thermal diffusion time scale at the carbon ignition depth. Fits to observed superburst lightcurves suggest that the ignition typically occurs at a column depth $y_{ign} = P/g \approx (0.5–2) \times 10^{12}$ g cm^{-2} (at $\rho \lesssim 10^9$ g cm^{-3}) that is smaller than the theoretical predictions described above.

The temperature profile $T(y)$ in Fig. 5 was calculated [53], taking into account the heat released from electron captures into excited states of daughter nuclei, with subsequent de-excitations of these nuclei. It produces additional heating of the crust that increases the crust temperature $T(y)$ and thus reduces the ignition density, in comparison with previous calculations. Nevertheless, the ignition densities are still larger than that inferred from observations even for the standard carbon burning rate. Therefore, the hindrance of the reaction rate makes reconciling theory with observations of superbursts even more difficult.

V. SUMMARY

We have investigated astrophysical consequences of a possible low-energy hindrance effect in carbon and oxygen fusion reactions [12] in dense matter.

We have briefly discussed (Sec. II) the effects of the hindrance on the ^{12}C+^{12}C, ^{12}C+^{16}O, and ^{16}O+^{16}O fusion rates in a wide range of densities and temperatures. We have shown that these effects strongly reduce the rates, as compared to the standard ones, at $T \lesssim (3–10) \times 10^8$ K. The reduction is especially dramatic at $\rho \gtrsim 10^9$ g cm^{-3} and $T \lesssim 3 \times 10^8$ K, particularly in the pycnonuclear regime.

We have studied the consequences of the proposed hindrance phenomenon for the nuclear evolution of massive late-type stars (Sec. III) and for carbon ignition in massive accreting white dwarfs (producing type Ia supernova explosions; Sec. IV A) and in accreting neutron stars (producing superbursts; Sec. IV B). In all these cases the hindrance effect is quite pronounced. In particular, it noticeably shifts the abundances of many isotopes in late-type stars, essentially increases the carbon ignition temperature $T_{ign}(\rho)$ in white dwarfs, and completely prevents carbon ignition in white dwarfs with an internal temperature $T \lesssim 2 \times 10^8$ K. It further complicates theoretical interpretation of observations of superbursts.

Let us stress that the hindrance effect in carbon and oxygen burning is not well established (Sec. II). It seems that experimentally measured low-energy fusion cross sections do not contradict this effect but they equally do not confirm it directly. More experimental and theoretical evidence is required to test it.

Moreover, our results for high densities and low temperatures are based on the extrapolation of the fusion cross sections to very low energies (Sec. II). Both S-factor extrapolations, the one based on the São Paulo potential model as well as the one based on the hindrance concept carry large uncertainties into the prediction of pycnonuclear burning rates. These uncertainties are typically associated with the theoretical treatment of the Coulomb tunneling problem (e.g., [1,2]).

Microscopic techniques based on the fermionic molecular dynamics [55] or two-center shell [56] models may provide improved theoretical tools for reducing the uncertainties of the present extrapolations.

We discussed only selected astrophysical consequences of the hindrance phenomenon; other consequences can also be important. In particular, the hindrance can affect the composition and thermal evolution of the inner crust of accreting neutron stars. The composition of this crust is determined by nuclear transformations of atomic nuclei under growing pressure produced by newly accreted material [57,58]. These transformations include pycnonuclear reactions between very neutron-rich nuclei in the inner crust, for instance, ^{34}Ne+^{34}Ne $\to^{68}$Ca at $\rho \approx 1.5 \times 10^{12}$ g cm^{-3} in the scenario of Ref. [57] (also see Ref. [59]). If these reactions are strongly blocked by the hindrance effect, the inner crust will possibly contain lighter nuclei than predicted with the standard S-factors. This may affect thermal energy release in the inner crust, which is thought to power sufficiently high thermal states of neutron stars in soft x-ray transients in quiescence between accretion episodes [60]. The idea of deep crustal heating in soft x-ray transients is potentially powerful to explore the physics of superdense matter in neutron star cores (as reviewed, e.g., in Refs. [61,62]).

All in all, the hindrance effect, if real, has important astrophysical consequences. A comparison of astrophysical predictions with observations may provide complementary data to direct laboratory measurements for testing the possibility of the hindrance effect in low-energy fusion cross sections.

[1] L. R. Gasques, A. V. Afanasjev, E. F. Aguilera, M. Beard, L. C. Chamon, P. Ring, M. Wiescher, and D. G. Yakovlev, Phys. Rev. C **72**, 025806 (2005).

[2] D. G. Yakovlev, L. R. Gasques, M. Beard, M. Wiescher, and A. V. Afanasjev, Phys. Rev. C **74**, 035803 (2006).

[3] C. A. Barnes, *Essays in Nuclear Astrophysics*, edited by C. A. Barnes, D. D. Clayton, and D. N. Schramm (Cambridge University Press, Cambridge, 1982), p. 193.

[4] L. Buchmann and C. A. Barnes, Nucl. Phys. **A777**, 254 (2006).

[5] W. A. Fowler, G. R. Caughlan, and B. A. Zimmerman, Annu. Rev. Astron. Astrophys. **13**, 69 (1975).

[6] G. R. Caughlan and W. A. Fowler, At. Data Nucl. Data Tables **40**, 283 (1988).

[7] C. L. Jiang *et al.*, Phys. Rev. Lett. **89**, 052701 (2002).

[8] C. L. Jiang, H. Esbensen, B. B. Back, R. V. F. Janssens, and K. E. Rehm, Phys. Rev. C **69**, 014604 (2004).

[9] C. L. Jiang *et al.*, Phys. Rev. Lett. **93**, 012701 (2004).

[10] C. L. Jiang *et al.*, Phys. Rev. C **71**, 044613 (2005).

[11] C. L. Jiang, B. B. Back, H. Esbensen, R. V. F. Janssens, and K. E. Rehm, Phys. Rev. C **73**, 014613 (2006).

[12] C. L. Jiang, K. E. Rehm, B. B. Back, and R. V. F. Janssens, Phys. Rev. C **75**, 015803 (2007).

[13] Ş. Mişicu and H. Esbensen, Phys. Rev. Lett. **96**, 112701 (2006).

[14] C. L. Jiang *et al.*, Phys. Lett. **B640**, 18 (2006).

[15] Ş. Mişicu and H. Esbensen, Phys. Rev. C **75**, 034606 (2007).

[16] J. R. Patterson, H. Winkler, and C. S. Zaidins, Astrophys. J. **157**, 367 (1969).

[17] M. G. Mazarakis and W. E. Stephens, Phys. Rev. C **7**, 1280 (1973).

[18] M. D. High and B. Cujec, Nucl. Phys. **A282**, 181 (1977).

[19] K. U. Kettner, H. Lorenz-Wirzba, and C. Rolfs, Z. Phys. A **298**, 65 (1980).

[20] H. W. Becker, K. U. Kettner, C. Rolfs, and H. P. Trautvetter, Z. Phys. A **303**, 305 (1981).

[21] K. A. Erb and D. A. Bromley, Phys. Rev. C **23**, 2781 (1981).

[22] B. Dasmahapatra, B. Cujec, and F. Lahlou, Nucl. Phys. **A384**, 257 (1982).

[23] L. J. Satkowiak, P. A. DeYoung, J. J. Kolata, and M. A. Xapsos, Phys. Rev. C **26**, 2027 (1982).

[24] P. Rosales *et al.*, Rev. Mex. Fís. **49** Supplement 4, 88 (2003).

[25] E. F. Aguilera *et al.*, Phys. Rev. C **73**, 064601 (2006).

[26] L. Barrón-Palos *et al.*, Nucl. Phys. **A779**, 318 (2006).

[27] T. Spillane *et al.*, Phys. Rev. Lett. **98**, 122501 (2007).

[28] W. Greiner, J. Y. Park, and W. Scheid, *Nuclear Molecules* (World Scientific, Singapore, 1994).

[29] B. Cujec and C. A. Barnes, Nucl. Phys. **A266**, 461 (1976).

[30] P. R. Christensen, Z. E. Switkowskiw, and R. A. Dayras, Nucl. Phys. **A280**, 189 (1977).

[31] H. Spinka and H. Winkler, Nucl. Phys. **A233**, 456 (1974).

[32] D. G. Kovar *et al.*, Phys. Rev. C **20**, 1305 (1979).

[33] G. Hulke, C. Rolfs, and H.-P. Trautvetter, Z. Phys. A **297**, 161 (1980).

[34] S.-C. Wu and C. A. Barnes, Nucl. Phys. **A422**, 373 (1984).

[35] J. Thomas, Y. T. Chen, S. Hinds, D. Meredith, and M. Olson, Phys. Rev. C **33**, 1679 (1986).

[36] A. Kuronen, J. Keinonen, and P. Tikkanen, Phys. Rev. C **35**, 591 (1987).

[37] E. E. Salpeter and H. M. Van Horn, Astrophys. J. **155**, 183 (1969).

[38] A. Chieffi, M. Limongi, and O. Straniero, Astrophys. J. **502**, 737 (1998).

[39] M. F. El Eid, B. S. Meyer, and L. S. The, Astrophys. J. **611**, 452 (2004).

[40] M. Limongi and A. Chieffi, Astrophys. J. **592**, 404 (2003).

[41] M. Limongi and A. Chieffi, Astrophys. J. **647**, 483 (2006).

[42] E. F. Brown and L. Bildsten, Astrophys. J. **496**, 915 (1998).

[43] A. Cumming and L. Bildsten, Astrophys. J. **559**, L127 (2001).

[44] W. Hillebrandt and J. Niemeyer, Annu. Rev. Astron. Astrophys. **38**, 191 (2000).

[45] S. E. Woosley, S. Wunsch, and M. Kuhlen, Astrophys. J. **607**, 921 (2004).

[46] I. Domínguez, P. Höflich, and O. Straniero, Astrophys. J. **557**, 279 (2001).

[47] I. Baraffe, A. Heger, and S. E. Woosley, Astrophys. J. **615**, L378 (2004).

[48] T. Strohmayer and E. F. Brown, Astrophys. J. **566**, 1045 (2002).

[49] E. F. Brown, Astrophys. J. **614**, L57 (2004).

[50] E. Kuulkers, Nucl. Phys. **B132** proceedings supplements, 466 (2004).

[51] N. N. Weinberg, L. Bildsten, and E. F. Brown, Astrophys. J. **650**, L119 (2006).

[52] H. Schatz, L. Bildsten, A. Cumming, and M. Ouelette, Nucl. Phys. **A718**, 247 (2003).

[53] S. Gupta, E. F. Brown, H. Schatz, P. Möller, and K.-L. Kratz, Astrophys. J. **662**, 1188 (2007).

[54] A. Cumming, J. Macbeth, J. J. M. in't Zand, and D. Page, Astrophys. J. **646**, 429 (2006).

[55] T. Neff, H. Feldmeier, and K. Langanke, arXiv:nucl-th/0703030v1.

[56] A. Diaz-Torres and W. Scheid, Nucl. Phys. **A757**, 373 (2005).

[57] P. Haensel and J. L. Zdunik, Astron. Astrophys. **229**, 117 (1990).

[58] P. Haensel and J. L. Zdunik, Astron. Astrophys. **404**, L33 (2003).

[59] D. G. Yakovlev, L. Gasques, and M. Wiescher, Mon. Not. R. Astron. Soc. **371**, 1322 (2006).

[60] E. F. Brown, L. Bildsten, and R. E. Rutledge, Astrophys. J. **504**, L95 (1998).

[61] D. G. Yakovlev and C. J. Pethick, Annu. Rev. Astron. Astrophys. **42**, 169 (2004).

[62] D. Page, U. Geppert, and F. Weber, Nucl. Phys. **A777**, 497 (2006).